Measurement and Error Evaluation of Electrical Parameters at Plasma Relevant Frequencies and Impedances

Craig Garvin,* Brian E. Gilchrist,† Dennis S. Grimard, and Jessy W. Grizzle

Abstract

The errors present in electrical measurements at frequencies and impedances relevant to plasma processing in the semiconductor industry are studied. A theoretical bound on calculated delivered power error as a function of measured electrical values is derived. The derivation shows that for constant measurement error, power error is a linear function of load impedance expressed in terms of voltage standing wave ratio. This bound is supported by experimental data taken with both a directional coupler and a voltage- and current- based probe. Linear and nonlinear model based sensing methods are implemented which reduce power error by a factor of five over a standard calibration. Published results are cited which indicate that the voltage standing wave ratio of typical plasma processing and experimental regimes is high enough to cause small measurement errors to result in large calculated power errors.

Nomenclature

electrical state: electrical state, no representation chosen

load: a one port network with a specific impedance or reflection coefficient, no representation chosen

probe: measured values taken at the probe's measurement ports

srp: 'sensor reference plane' the reference plane inside the sensor where measurement actually takes place. See Section 6.1

lrp: 'load reference plane'- the reference plane at the point in the circuit where a load is connected to the probe. See Figure 6

x_{ref} **:** electrical state at *ref* point in circuit, no representation chosen

$(\mathbf{V}^+, \mathbf{V}^-)$ **:** electrical state *represented* as forward and reverse voltage waves

$(\mathbf{v}, \mathbf{i})$ **:** electrical state *represented* as current and voltage

'(var**)- based' :** electrical state *measured* as 'var'

var **:** *actual* value of var

$\overline{var}$ **:** *measured* value of var

$\widehat{var}$ **:** *estimated* value of var

ϵ_{var} **:** *relative* error in var as $\epsilon_{var} = \frac{\overline{var} - var}{var}$

Δ_{var} **:** *absolute* error in var as $\Delta_{var} = \overline{var} - var$

$\mid var \mid$ **:** absolute value of var (*rms* if time varying)

$var^\star$ **:** complex conjugate of var

$\Re(var)$ **:** real part of var

$\Im(var)$ **:** imaginary part of var

P_{ref} **:** power at *ref* point in circuit

$\mathbf{V}^+_{ref}$ **:** complex value of forward voltage at *ref* point in circuit

$\mathbf{V}^-_{ref}$ **:** complex value of reverse voltage at *ref* point in circuit

$\mathbf{\Gamma}_{ref}$ **:** complex reflection coefficient at *ref* point in circuit

$\phi_{\Gamma_{ref}}$ **:** phase angle of reflection coefficient at *ref* point in circuit

$\mathbf{v}_{ref}$ **:** complex value of voltage at *ref* point in circuit

$\mathbf{i}_{ref}$ **:** complex value of current at *ref* point in circuit

$\mathbf{Z}_{ref}$ **:** complex impedance at *ref* point in circuit

$\theta_{Z_{ref}}$ **:** phase angle of impedance at *ref* point in circuit

S_{dut} **:** scattering matrix of device under test *dut*

s_{rc} **:** scattering parameter *r,c* of scattering marix

A_{dut} **:** ABCD matrix of device under test *dut*

1 Introduction

In semiconductor manufacturing applications, RF powered plasma processes are typically driven at $13.56 MHz$. It has been well known since the early days of plasma processing that the power delivered to the plasma is a dominant factor affecting processing. More recent published data [1–4] indicates that anywhere between 10% and 90% of the input power is dissipated outside the plasma discharge. Such a finding motivates using the delivered power and not the generator power as the control input in plasma processing, as done by [5, 6]. Clearly, controlling the delivered power requires determining this value with small enough errors that using measured delivered power as a feedback variable actually improves performance.

*C. Garvin, D. Grimard, and J. Grizzle are with the University of Michigan Electronics Manufacturing Laboratory, 3300 Plymouth Rd., Ann Arbor, MI 48105-2108

†Brian E. Gilchrist is with the University of Michigan Radiation Laboratory, 1301 Beal Ave. Ann Arbor, MI 48109-2122

Another goal of measuring plasma electrical parameters is to reconstruct physical plasma quantities from these electrical measurements. Many researchers [1, 7–13] have proposed models relating plasma physics to observed impedance. Although varying in the specifics, most agree that the plasma sheath can be represented by a capacitor, and the rate of dissociation of electrons from atoms as a resistor. If we seek to determine the plasma parameters from measured electrical parameters, then error free electrical measurements are also desired.

It has long been known that the plasma acts as a nonlinear load, to some degree rectifying the input frequency and resulting in a DC offset and harmonics of the fundamental frequency. Recently, Klick [14] has proposed a model for interpreting these higher harmonics as additional indicators of the plasma's physical state. It is likely that whatever challenge exists in measuring the plasma electrical state at $13.56 MHz$ is exacerbated at higher harmonics of this frequency. This follows from the observation that the major sources of error: losses, radiation, and reference plane changes all become increasingly prominent as frequency increases.

Numerous measurements of plasma electrical parameters have been published [3, 12, 15–20]. All of these note the measurement equipment used and describe the calibration methodology implemented. Clearly, small errors in measuring electrical parameters such as $(\mathbf{V}^+, \mathbf{V}^-)$ or $(\mathbf{v}, \mathbf{i})$ are essential to determinating delivered power and plasma impedance with small errors. This paper addresses power and impedance measurement at plasma relevant frequencies and impedances. A theoretical derivation of power error as a function of measurement error is presented. Power error is shown to be a linear function of voltage standing wave ratio for constant measurement error. Experimental data is presented to support the theoretical limit.

Relatively high errors in P_{lrp} (power at the load reference plane) are observed even under benign test conditions. Sections 5.2 and 6.3 develop methods for reducing the error of RF probes by model based sensing. Tests of two high power probes are presented representing a typical directional coupler and voltage and current based probe. To minimize errors, experiments are performed at a single frequency and very low power on simulated plasma loads. Extension to actual plasmas and plasma-relevant power levels is straight forward. Additional results covering real time and high power compatible data acquisition systems will be covered in a subsequent paper.

2 Microwave and Network Theory Summary

This section summarizes the basic microwave and network theory needed to read this paper, as the experimental work and results presented in this paper rely upon these concepts. The material is derived from [21] and can be obtained from any standard text in microwave engineering. As a simplification, all equations assume a constant characteristic impedance ($Z_\circ$) throughout the circuit.

The electrical quantities in a circuit will be referred to as the '*electrical state*' at a '*reference plane*'. The electrical state refers the specification of either complex current and voltage, $(\mathbf{v}, \mathbf{i})$, or complex forward and reverse voltage waves, $(\mathbf{V}^+, \mathbf{V}^-)$. A reference plane is a plane perpendicular to the direction of power flow in a circuit at which electrical state can be specified. One of the main reference planes we will use is the load reference plane. This reference plane refers to the point in the circuit where a load is connected to the probe system, as seen in Figure 6. In all equations, if no reference plane is specified, then the equation is true as long as all variables are at the same reference plane. Both voltage, current and forward, reverse voltage representation of electrical state are used, related by (1).

$$\begin{bmatrix} \mathbf{v} \\ \mathbf{i} \end{bmatrix} = \begin{bmatrix} 1 & 1 \\ \frac{1}{Z_\circ} & -\frac{1}{Z_\circ} \end{bmatrix} \cdot \begin{bmatrix} \mathbf{V}^+ \\ \mathbf{V}^- \end{bmatrix} \quad (1)$$

The following derived quantities are obtained for power being delivered at a particular reference plane in a circuit.

$$P = \frac{|\mathbf{V}^+|^2 - |\mathbf{V}^-|^2}{Z_\circ} \quad (2)$$

$$P = \Re(v \cdot i^\star) \quad (3)$$

Note that all electrical quantities are specified as *rms* values, so no factor of $\frac{1}{2}$ is required in power calculation

$$\text{VSWR} = \frac{1 + |\mathbf{\Gamma}|}{1 - |\mathbf{\Gamma}|} \quad (4)$$

$$\mathbf{Z} = \frac{\mathbf{v}}{\mathbf{i}} \quad (5)$$

$$\mathbf{\Gamma} = \frac{\mathbf{V}^-}{\mathbf{V}^+} \quad (6)$$

$$\mathbf{\Gamma}_{load} = \frac{\mathbf{Z}_{load} - Z_\circ}{\mathbf{Z}_{load} + Z_\circ} \quad (7)$$

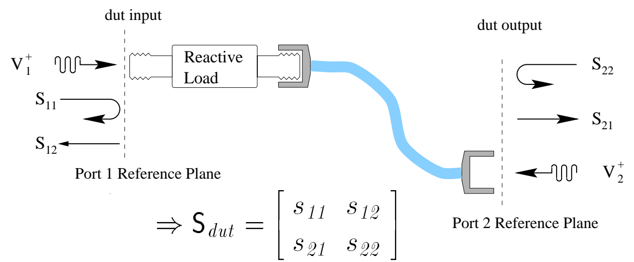

Figure 1: Determining the scattering parameters of a two port network

Two port representations are used to identify network elements and to transform between reference planes. The scattering matrix is used for direct identification of a network. Figure 1 shows a typical application. The device under test, *dut*, is connected between the two ports of the vector network analyzer which measures the scattering matrix: S_{dut}. The scattering matrix relates forward and reverse voltages according to (8).

$$\begin{bmatrix} \mathbf{V}_1^- \\ \mathbf{V}_2^- \end{bmatrix} = \begin{bmatrix} s_{11} & s_{12} \\ s_{21} & s_{22} \end{bmatrix} \cdot \begin{bmatrix} \mathbf{V}_1^+ \\ \mathbf{V}_2^+ \end{bmatrix} \quad (8)$$

Transforming between reference planes is achieved with the ABCD matrix, as shown in Figure 2. The ABCD matrix is uniquely determined by S_{dut} and allows the voltage and current at two reference planes to be related by (9).

$$\begin{bmatrix} v_1 \\ i_1 \end{bmatrix} = \begin{bmatrix} A & B \\ C & D \end{bmatrix} \cdot \begin{bmatrix} v_2 \\ i_2 \end{bmatrix} \tag{9}$$

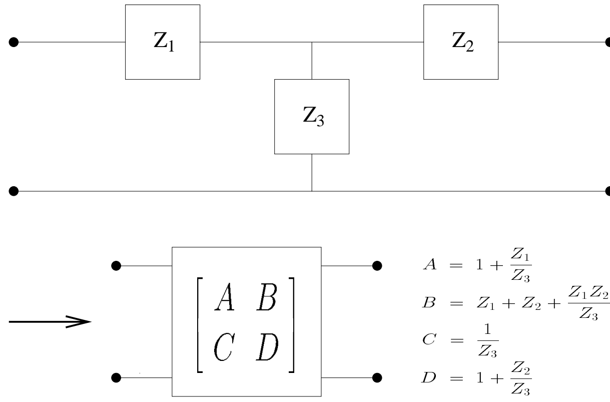

Figure 2: T Network Representation of a Two Port Network

Given a two port reciprocal network, its behavior is uniquely determined by a three impedance T-network, also shown in Figure 2. When a load $\mathbf{Z}_{load}$ is connected at the output port, the impedance seen at the input port is given by (10).

$$\mathbf{Z}_{input} = \mathbf{Z}_1 + \frac{\mathbf{Z}_3(\mathbf{Z}_2 + \mathbf{Z}_{load})}{\mathbf{Z}_2 + \mathbf{Z}_3 + \mathbf{Z}_{load}} \tag{10}$$

We thus can determine the impedances that make up the T-network by connecting three different loads to the output of the two port network and solving a system of three equations for the uknown impedances $\mathbf{Z}_1$, $\mathbf{Z}_2$ and $\mathbf{Z}_3$.

3 Power Sensitivity Relation

It is possible to derive a simple expression for relative power error, (ϵ_P) as a function of voltage standing wave ratio (VSWR) and error in forward and reverse voltage ($\epsilon_{\mathbf{V}^+}$, $\epsilon_{\mathbf{V}^-}$). A similar relationship between relative power error and electrical state measured as voltage and current exists, though it is more tedious to derive. A numerical simulation will show that in the ($\mathbf{v}$, $\mathbf{i}$) case, the sensitivities are effectively the same.

Relative power error is defined in (11)

$$\epsilon_P = \frac{\overline{P} - P}{P} \tag{11}$$

$\overline{P}$ is the measured power based on the measured electrical state, including errors, and P is the actual power based on the exact electrical state. We see that when power is calculated from ($\mathbf{V}^+$, $\mathbf{V}^-$), as in (2), power is only a function of the magnitude of the measured state and not the phase. It follows naturally to seek a relationship between power error and VSWR, also a scalar quantity.

We define measurement error as follows: The measurement errors are fixed values: $\Delta_{|\mathbf{V}^+|}$ and $\Delta_{|\mathbf{V}^-|}$ independent of the magnitude of measured quantity. It is obvious that as the ratio of $\Delta_{|\mathbf{V}^+|}$ to $|\ \mathbf{V}^+\ |$ changes, so do errors in power. Accordingly, it is reasonable to derive a relationship between measurement errors and power errors for a fixed ratio of $\Delta_{|\mathbf{V}^+|}$ to $|\ \mathbf{V}^+\ |$ defined in (12).

$$\epsilon_{|\mathbf{V}^+|} = \frac{\Delta_{|\mathbf{V}^+|}}{|\ \mathbf{V}^+\ |} \tag{12}$$

Similarly a second variable is used for to describe error in $|\ \mathbf{V}^-\ |$ where $\epsilon_{|\mathbf{V}^-|}$ is defined in (13).

$$\epsilon_{|\mathbf{V}^-|} = \frac{\Delta_{|\mathbf{V}^-|}}{|\ \mathbf{V}^+\ |} \tag{13}$$

We now derive the relationship between measurement error in ($\mathbf{V}^+$, $\mathbf{V}^-$) and power error as parameterized by VSWR. The actual power is given by (2). By including error terms in the measurement, we can calculate power including error as (14).

$$\begin{aligned} \overline{P} &= P + \Delta_P \\ \overline{P} &= \frac{(|\ \mathbf{V}^+\ | + \Delta_{|\mathbf{V}^+|})^2 - (|\ \mathbf{V}^-\ | + \Delta_{|\mathbf{V}^-|})^2}{Z_\circ} \end{aligned} \tag{14}$$

Substituting (12), (13), and (6) into (14) allows us to calculate an algebraic expression for power error (15)

$$\epsilon_P = \frac{2\epsilon_{|\mathbf{V}^+|} + \epsilon^2_{|\mathbf{V}^+|} - |\ \mathbf{\Gamma}\ |^2\ (2\epsilon_{|\mathbf{V}^-|} + \epsilon^2_{|\mathbf{V}^-|})}{1 - |\ \mathbf{\Gamma}\ |^2} \tag{15}$$

A further simplification is achieved by substituting for $|\ \mathbf{\Gamma}\ |$ using (4). The result given in (16) appears a bit cumbersome but several simplifications are possible.

$$\begin{aligned} \epsilon_P \quad = \quad & \frac{(1+\text{VSWR})^2}{4\text{VSWR}}(2\epsilon_{|\mathbf{V}^+|} + \epsilon^2_{|\mathbf{V}^+|}) \\ & + \frac{(1-\text{VSWR})^2}{4\text{VSWR}}(2\epsilon_{|\mathbf{V}^-|} + \epsilon^2_{|\mathbf{V}^-|}) \end{aligned} \tag{16}$$

We note that typical error terms $\epsilon_{|\mathbf{V}^+|}$ and $\epsilon_{|\mathbf{V}^-|}$ are very small, thus higher powers of these terms can be neglected. Additionally, we are interested in the limit as VSWR $\gg 1$. Under these conditions parts of (16) become (17).

$$\frac{(1 \pm \text{VSWR})^2}{4\text{VSWR}} \Rightarrow \pm\frac{1}{4}\text{VSWR} \tag{17}$$

As a final simplification we note that at high VSWR, ϵ_P is a function of the difference between $\epsilon_{|\mathbf{V}^+|}$ and $\epsilon_{|\mathbf{V}^-|}$. If we define $\epsilon_{|V|} = \epsilon_{|\mathbf{V}^+|} - \epsilon_{|\mathbf{V}^-|}$ we obtain the very simple relationship given in (18).

$$\epsilon_P = \text{VSWR} \cdot \frac{\epsilon_{|V|}}{2} \tag{18}$$

We see from (18) that for a constant difference in measurement error, the error in power is a linear function of the load mismatch expressed as VSWR.

Deriving a similar expression for the relation between ϵ_P and ($\mathbf{v}$, $\mathbf{i}$) is tedious. However, numerical simulation indicates that a similar sensitivity exists. In order to perform the simulation, the exact test conditions must be specified. As in the ($\mathbf{V}^+$, $\mathbf{V}^-$) case

we assume that the measurement device has an error expressed as Δ_x. Unlike the $(\mathbf{V}^+, \mathbf{V}^-)$ case, it is normal for the values of $\mid \mathbf{v} \mid$, $\mid \mathbf{i} \mid$, and θ_Z to move substantially as a function of load impedance, so it is more difficult to find an expression like (12). The following simulation is performed. A single value of $\mid \mathbf{V}^+ \mid$ is used. 100 values of $\mid \mathbf{V}^- \mid$ are generated corresponding to VSWR 's from 1 to 100, using 4 and 6. Each value of $\mid \mathbf{V}^+ \mid$ and $\mid \mathbf{V}^- \mid$ is converted to 360 pairs of $(\mathbf{v}, \mathbf{i})$ by using values of ϕ_Γ from 1 to 360°. These values of $(\mathbf{v}, \mathbf{i})$ correspond to the same VSWR but different Z. We can now introduce a simulated measurement error in $\mid \mathbf{v} \mid$, $\mid \mathbf{i} \mid$, and θ_Z and determine the power error resulting from the measurement error for the different values of $(\mathbf{v}, \mathbf{i})$ at a constant VSWR. The maximum ϵ_P at each VSWR is then plotted. Figure 3 shows the simulated result of a 1% error in $\mid \mathbf{v} \mid$ $\mid \mathbf{i} \mid$ and θ_Z on ϵ_P, as well as plotting (16) for a $+1\%$ $\epsilon_{|\mathbf{V}^+|}$ and -1% $\epsilon_{|\mathbf{V}^-|}$. Two conclusions can be drawn from Figure 3. First, that the simplified relationship predicted by (18) accurately captures the exact behavior of ϵ_P as a function of VSWR in $(\mathbf{V}^+, \mathbf{V}^-)$- based measurement. Second, the same linear relationship as predicted by (18) is seen in $(\mathbf{v}, \mathbf{i})$-based measurement, but with a slightly lower gain factor.

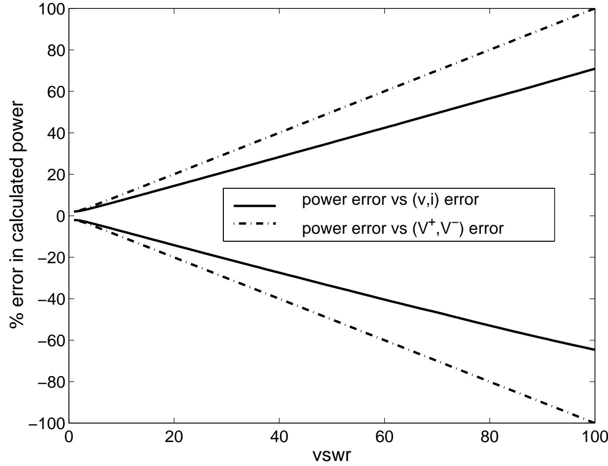

Figure 3: Effect of 1% measurement error on ϵ_P as a function of VSWR

In both $(\mathbf{V}^+, \mathbf{V}^-)$ and $(\mathbf{v}, \mathbf{i})$ case, any magnitude of measurement error can result in zero power error, if the errors exactly cancel. It is clear that such a scenario is exceedingly unlikely. Figure 3 is based on the assumption that measurement is a constant Δ_x, independent of the magnitude of measured signal. It is clear that if errors in $\mid \mathbf{v} \mid$ and $\mid \mathbf{i} \mid$ are in terms of a constant fraction of the measured value, then their contribution will be essentially inconsequential, and phase error will be the only factor affecting power error.

Power error sensitivity to VSWR is small if the plasma load has a low VSWR. Table 1 shows load VSWR calculated from published values of measured impedance in plasma cells. In all cases, VSWR is calculated from published direct measurements, without 'de-embedding'. We see from Table 1 that the range of published plasma load VSWR's is extremely wide. As a result, the measurement errors required for low error power calculation, as calculated from (18) varies from being easily attainable with factory type equipment to requiring the most precise laboratory equipment and test conditions. It is of interest, therefor to determine whether the theoretical prediction of (18) bear out in practice. This is addressed in Section 5

Table 1: Load VSWR calculated from published values of plasma impedance

power	Press	Gas	vswr	source
50 W	100 mT	Ar	7.22	[16]
500 W	100 mT	Ar	47.4	[16]
200 Vpp	100 mT	Ar	67.6	[19]
800 W	50 mT	O_2	4.21	[9]
800 W	400 mT	O_2	5.82	[9]
125 W	700 mT	CF_4	1007	[3]
200 Vpp	100 mT	Ar	78.38	[18]
100 W	15 mT	Ar	14.9	[17]
50 W	50 mT	Ar	57.6	[13]
50 W	3 mT	Ar	303.6	[1]
50 W	300 mT	Ar	98.0	[1]
100 W	400 mT	Cl_2	19.6	[22]

4 Experimental Setup

It is clear that any work on measurement error must be comparative. We can compare the measurements given by our system either to theoretical predictions or to better measured values. Although it might be possible to determine the theoretical impedance values from exact analysis, it is very unlikely that we can make theoretical predictions about power levels. A somewhat less satisfying but more reasonable course of action is to use an agreed upon reference instrument as the source of 'actual' values. Such an instrument is a research grade vector network analyzer. Testing with a vector network analyzer mandates using very low powers and working with simulated plasma loads. Additionally, to reduce the number of experiments, all experiments are at a single frequency, $13.56MHz$.

4.1 Equipment

Our reference is a Hewlett Packard 8753B vector network analyzer, calibrated with a Hewlett Packard 8732B type N calibration kit. This is a representative research grade analyzer. The experimental data presented in this paper compares two classes of probes. One is a directional coupler-based probe, the other is the more familiar voltage and current-based probe. A directional coupler is an electromagnetic device which samples a small portion of the forward and reverse waves in a transmission line, separates the waves and sends the greatly attenuated waves to two measurement ports: forward and reverse. A Werlatone C1373 $1.5MHz$ to $80MHz$ directional coupler rated at 750 Watts power with a nominal $-30dB$ coupling between main line and sensor ports is used. The other probe is the more familiar combina-

tion of voltage and current probe. The voltage probe is simply a resistive voltage divider that produces an output proportional to $\frac{1}{300}$ of the voltage at the sensor. The current probe uses an inductively coupled coil to produce a voltage output proportional to $\frac{1}{60}$ of the current. We use a voltage and current sensor packaged with type N connectors sold by Fourth State Technologies.

4.2 Test Loads

As derived in (18), load VSWR is expected to greatly determine the effect of measurement accuracy on power accuracy. To test this theory, we designed loads in 5 VSWR classes: 1, 3, 8.66, 25 and 75. We are interested also in measuring the same load VSWR at different ϕ_Γ. Accordingly, each load VSWR was achieved with four different ϕ_Γ: high impedance capacitive, low impedance capacitive, low impedance inductive and high impedance inductive. Test loads meeting these specifications can be built by using either inductors or capacitors in series or parallel with the 50Ω resistive load. Inductors are custom wound on toroidal iron cores. These can be adjusted for exact reactance by changing the inter - coil spacing. Desired capacitance is achieved by combining a standard 1000 Volt breakdown ceramic capacitor with Voltronic adjustable capacitors for fine tuning.

4.3 Assumptions

It is valuable to review the assumptions under which the experiments described in this paper are performed.

1. We assume that once calibrated, the network analyzer exactly measures relative quantities, and that these values are the actual values of electrical parameters.

2. We assume that we can compose circuit elements according to network theory. That is, given that a load has an impedance $\mathbf{Z}_{load}$ and a length of cable is represented by the scattering matrix S_{cable}, then the impedance of the load through the cable is a known single valued function of S_{cable} and $\mathbf{Z}_{load}$.

3. We assume that results obtained at these test powers are closely related to results at plasma relevant powers.

4. We assume that all measurements have effectively perfect precision. Differences between measured and actual values are due solely to the type of load used in the experiment.

4.4 Experimental Method

We would like to evaluate the accuracy of our probes under strictly controlled test circumstances. Accordingly, the following experiment is constructed. We use an HP 8753B vector network analyzer as a source, receiver and reference by making use of two different measurement configurations. Figure 4 shows the analyzer configured in *reference mode*. In this configuration, the actual electrical states at port #1 and #2 of the vector network analyzer can be determined as well as S_{dut} where *dut* is the network composed of a series of two networks: the probe and probe cable, referred to as the *'probe system'* or *'prob_sys'*, and reactive load, and load cable, referred to as *'xload'*. As indicated in section 4.3, we assume that the electrical state as measured by the network analyzer is in fact the exact actual value of electrical state.

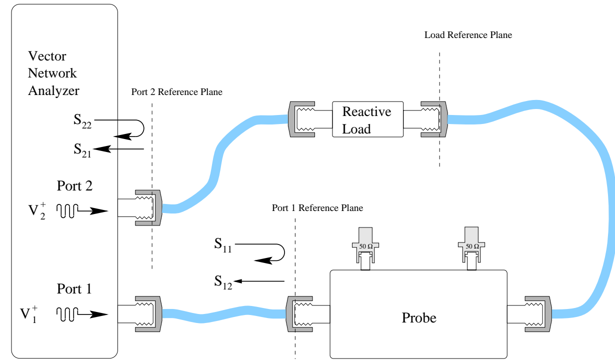

Figure 4: vector network analyzer configured in reference mode

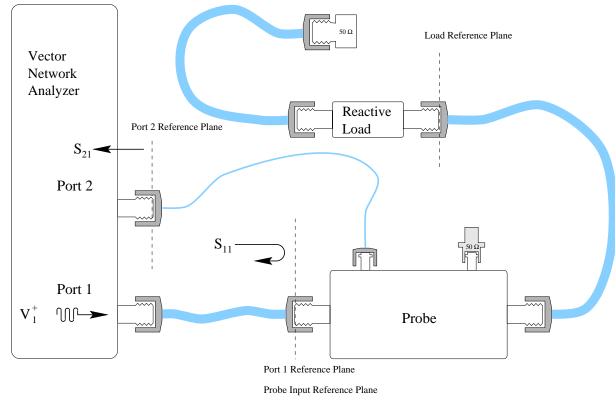

Figure 5: vector network analyzer configured in measurement mode

Figure 5 shows the analyzer configured in *measurement mode*. By terminating the reactive load with a matched load, the electrical state in the *dut* is identical to that of the reference mode, but now port #2 of the vector network analyzer is available to receive the output of the probe. We can use the s_{21} measurement taken in this manner as the most accurate method of measuring the probe output as a function of load. In this configuration, the *probe* provides us with the measurement of the electrical state and the network analyzer acts as the data acquisiton system for the probe.

For each different load, three measurements are taken. One measurement in reference mode is used to determine S_{dut}. From this scattering matrix, we determine the two port characteristics of the combined *probe system* and *xload*. We then switch to measurement mode, and connect $\overline{\mathbf{V}^+}$ or $\overline{\mathbf{v}}$ output of the probe (depending on the probe used) to port #2 of the analyzer, and terminate the other probe output with a matched load. A second measurement is made with the $\overline{\mathbf{V}^-}$ or $\overline{\imath}$ port of the probe connected to port #2 of the vector network analyzer. These measurements gives us $\overline{x_{probe}}$, the electrical state measured by the probe, as received by the network analyzer. In the following

sections, *actual values*: $\mathbf{V}^+$, $\mathbf{V}^-$, $\mathbf{v}$, and $\mathbf{i}$ refer to values derived from network analyzer measurements in *reference mode*. *Measured values*: $\overline{\mathbf{V}^+}$, $\overline{\mathbf{V}^-}$, $\overline{\mathbf{v}}$, $\overline{\imath}$ refer to values obtained from the probe using the network analyzer in *measurement mode*. We will discuss how to calibrate these value and how to compare them to the actual state as determined by the vector network analyzer in Sections 4.5 and 4.6.

4.5 Standard Probe Calibration

It is standard practice to assume that the output of the probe is related to the electrical state by a simple multiplication factor, or calibration factor. For both systems, we calibrate the gain relative to the load reference plane, which is the end of the probe cable. The calibration is achieved by comparing the actual state at load reference plane to the measured output of the probe for a properly chosen test point. Because all the measurements done by the vector network analyzer are relative, we can assume the source generates $\mathbf{V}^+_{source} = 1$ Volt. Thus, all S-parameters can be interpreted directly as voltages. We determine the actual state at the load reference plane by making the *dut* the *probe system*. In this manner, $\mathbf{V}^+_{lrp} = s_{21}$ and $\mathbf{V}^-_{lrp} = 0$ (because port #2 of the vector network analyzer is matched). The state can be converted to $(\mathbf{v}, \mathbf{i})$ as needed, using (1).

Calibrating the directional coupler is a bit cumbersome because the matched termination does not generate a $\mathbf{V}^-$ and thus cannot be used to calibrate the $\mathbf{V}^-$ gain. In order to calibrate the forward gain, we make measurements in *reference mode* and *measurement mode* to obtain (19)

$$\begin{aligned} \mathbf{V}^+_{lrp} &= s_{21} \\ &\quad \text{(analyser measurement is actual } \mathbf{V}^+_{lrp}) \\ \overline{\mathbf{V}^+_{probe}} &= s_{21} \\ &\quad \text{(analyser measures probe output)} \\ K_{\mathbf{V}^+} &= \frac{\mathbf{V}^+_{lrp}}{\overline{\mathbf{V}^+_{probe}}} \end{aligned} \tag{19}$$

Calibrating the reverse gain is achieved by reversing the direction of power flow through the probe and repeating the process.

$$\begin{aligned} \mathbf{V}^-_{lrp} &= s_{12} \\ &\quad \text{(analyser measurement is actual } \mathbf{V}^-_{lrp}\ ) \\ \overline{\mathbf{V}^-_{probe}} &= s_{12} \\ &\quad \text{(analyser measures probe output)} \\ K_{\mathbf{V}^-} &= \frac{\mathbf{V}^-_{lrp}}{\overline{\mathbf{V}^-_{probe}}} \end{aligned} \tag{20}$$

The rationale for this measurement is to reproduce the physical conditions of actual operation. The $\mathbf{V}^+$ originates upstream of the load and passes through probe first, and then the load. Thus any losses between these points will be seen by the load but not the probe. The situation for $\mathbf{V}^-$ is opposite. The reflected wave is generated at the load reference plane, thus any losses between load and probe will be seen by the probe but not by the load.

Determining the current and voltage calibration is actually easier than the calibration for the directional coupler, as shown in (21).

$$\begin{aligned} \begin{bmatrix} \mathbf{v}_{lrp} \\ \mathbf{i}_{lrp} \end{bmatrix} &= \begin{bmatrix} 1 & 1 \\ \frac{1}{Z_\circ} & -\frac{1}{Z_\circ} \end{bmatrix} \cdot \begin{bmatrix} s_{21_r} \\ 0 \end{bmatrix} \\ \overline{\mathbf{v}_{probe}} &= s_{21_m} \\ \overline{\imath_{probe}} &= s_{21_m} \\ s_{21_r} &= \text{reference mode value of } s_{21} \\ s_{21_m} &= \text{measurement mode value } s_{21} \end{aligned} \tag{21}$$

From the actual and measured values we can determine the proper gains:

$$\begin{aligned} K_{\mathbf{v}} &= \frac{\mathbf{v}_{lrp}}{\overline{\mathbf{v}_{probe}}} \\ K_{\mathbf{i}} &= \frac{\mathbf{i}_{lrp}}{\overline{\imath_{probe}}} \end{aligned} \tag{22}$$

The results of (19),(20), or (22) are taken as the standard calibration of the probe.

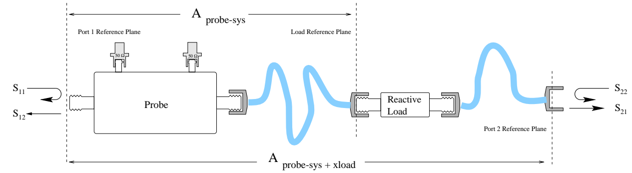

Figure 6: Determining Electrical State at load reference plane

4.6 Comparing Measured and Actual Electrical State

We would like to compare the measured electrical state given by the probe to the actual electrical state based on vector network analyzer S-parameters in order to determine the measurement error of the probe. If the *xload* is connected to the *probe system*, direct access to the electrical state at the load reference plane is blocked, as indicated in Figure 4. If the ABCD matrix of the *xload* only, A_{xload}, is known then the electrical state at port #2 can be transformed to the electrical state at the load reference plane via (23).

$$\begin{bmatrix} \mathbf{v}_{lrp} \\ \mathbf{i}_{lrp} \end{bmatrix} = \mathsf{A}_{xload} \cdot \begin{bmatrix} 1 & 1 \\ \frac{1}{Z_\circ} & -\frac{1}{Z_\circ} \end{bmatrix} \cdot \begin{bmatrix} \mathsf{S}_{21} \\ 0 \end{bmatrix} \tag{23}$$

A_{xload} is obtained from the ABCD matrix of the *probe system*, A_{prob_sys}, and ABCD matrix of the combined *probe system* and *xload*, $\mathsf{A}_{prob_sys+xload}$, as follows from (24).

$$\begin{aligned} \mathsf{A}_{prob_sys+xload} &= \mathsf{A}_{prob_sys} \cdot \mathsf{A}_{xload} \\ \mathsf{A}_{xload} &= \mathsf{A}^{-1}_{prob_sys} \cdot \mathsf{A}_{prob_sys+xload} \end{aligned} \tag{24}$$

Once A_{xload} is obtained for each test load, the actual values of $(\mathbf{v}, \mathbf{i})$ at the load reference plane are generated using (9) with

A_{xload}. Determining the measured electrical state is simply a function of obtaining two values of S_{21} in measurement mode and applying the gains determined in (19), (20), or (22). The physical networks corresponding to the ABCD matrices in (24) are shown in Figure 6

5 Results of Electrical State Measurement

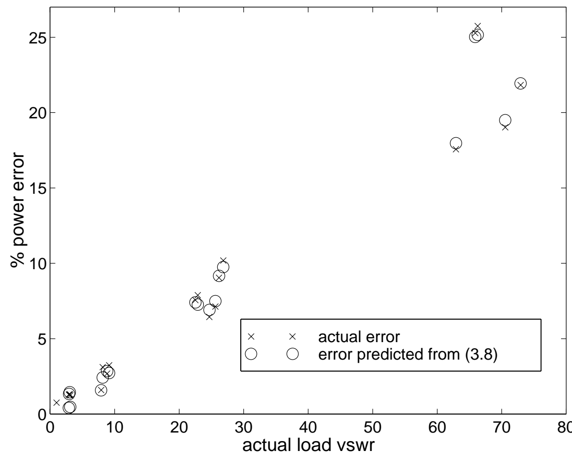

Figure 7: ϵ_P comparing $\overline{P_{probe}}$ to P_{lrp} using Directional Coupler and HP8753 vector network analyzer

5.1 Comparing Measured State using Standard Calibration to Actual Electrical State

Using the methodology described in Section 4.6, we can compare the actual electrical state at the load reference plane to the measured electrical state given by the probe's output as received by the vector network analyzer. Error in power, ϵ_P, is calculated using 11, where P is calculated from 2 or 3. A predicted power error is calculated using (18) where $\epsilon_{|V|}$ is given by (25)

$$\epsilon_{|V|} = \frac{(\overline{|\mathbf{V}^+|} - |\mathbf{V}^+|) - (\overline{|\mathbf{V}^-|} - |\mathbf{V}^-|)}{|\mathbf{V}^+|} \qquad (25)$$

To calculate $\epsilon_{|V|}$ in the $(\mathbf{v},\ \mathbf{i})$ based case, we convert $\overline{\mathbf{v}}$, $\overline{\imath}$ to $\overline{|\mathbf{V}^+|}$, $\overline{|\mathbf{V}^-|}$ using (1).

Figures 7 and 8 shows the power accuracy for the $(\mathbf{V}^+, \mathbf{V}^-)$ and $(\mathbf{v},\ \mathbf{i})$-based measurement. We see that actual power accuracy closely matches the predicted accuracy calculated from (18) for both cases. We also note that there is substantial power error even under these very controlled circumstances. Clearly, measurement interpretation beyond the simple calibration of Section 4.5 is needed.

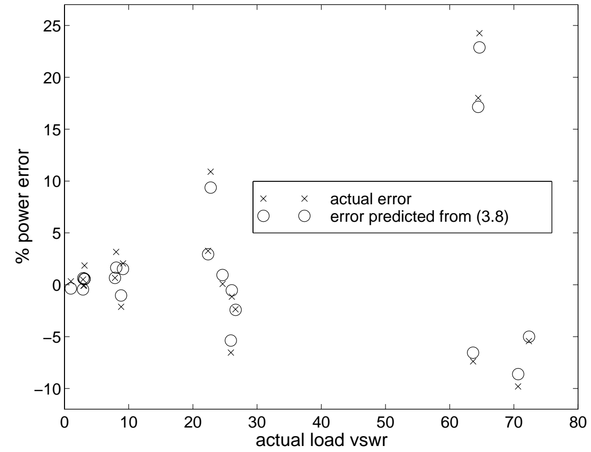

Figure 8: ϵ_P comparing $\overline{P_{probe}}$ to P_{lrp} using current and voltage probe and HP8753 vector network analyzer

5.2 Comparing Measured and Actual Electrical State Using Deembedding

The reason for the errors seen in Figure 7 should be clear. We are measuring the electrical state at the probe, but we desire the electrical state at the load reference plane. Clearly, there are losses between these points and these losses transform into measurement error. The measured power is higher than the actual power because some of the measured power is dissipated in the probe and cable and not the load. We can correct this problem by creating a model of the network between the load reference plane and the probe's output values. This makes use of the relatively common 'de-embedding' process described in [3, 13, 17, 19]. By connecting a known load to the load reference plane and measuring the electrical state as determined by the probe, we can determine the intermediate electrical network that corresponds to the relation between the electrical state given by the probe and the actual electrical state at the load. Once we

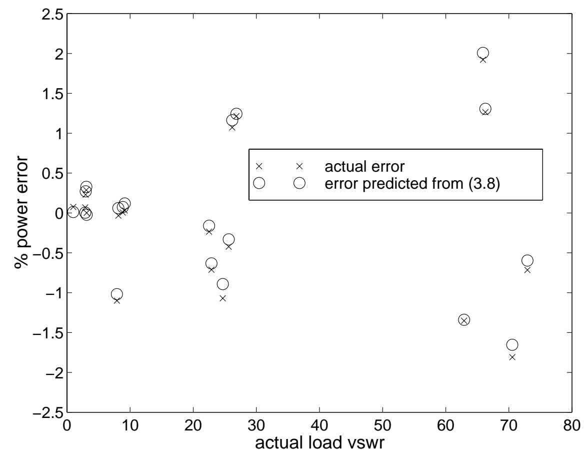

Figure 9: ϵ_P comparing $\widehat{P_{probe}}$ to P_{lrp} using Directional Coupler and HP8753 vector network analyzer

have determined $\mathbf{Z}_{probe}$ of the actual impedances, a set of three equations can be solved for the impedances of the T-network equivalent circuit between probe and load reference plane. This network is converted to the ABCD matrix $\mathsf{A}_{\overline{probe}}$. Using (26) gives the de-embedded values.

$$\begin{bmatrix} \widehat{\mathbf{v}_{lrp}} \\ \widehat{\imath_{lrp}} \end{bmatrix} = \mathsf{A}_{\overline{probe}}^{-1} \cdot \begin{bmatrix} \overline{\mathbf{v}_{lrp}} \\ \overline{\imath_{lrp}} \end{bmatrix} \quad (26)$$

For the test with de-embedding, we prepare the data in the same manner as in Section 5.1, and perform the same comparison to predicted power error based on (18). Figures 9 and 10 show that the results of de-embedding with the directional coupler are excellent, whereas those with the voltage and current probe are not nearly as good. With the directional coupler, de-embedding reduces the power error from $+25\%$ total to $\pm 2\%$. With the voltage and current probe, the trend in the power error is removed by de-embedding, but a sizeable scatter remains. In both cases, the predicted power error very accurately matches the actual power error. We can thus conclude that measurement error has been reduced by a factor of 6 in $(\mathbf{V}^+, \mathbf{V}^-)$ mode, but only about 50% in $(\mathbf{v}, \mathbf{i})$ mode. In order to explain this difference as well as reduce the error of $(\mathbf{v}, \mathbf{i})$ based measurement, a more sophisticated data analysis and error correction is needed.

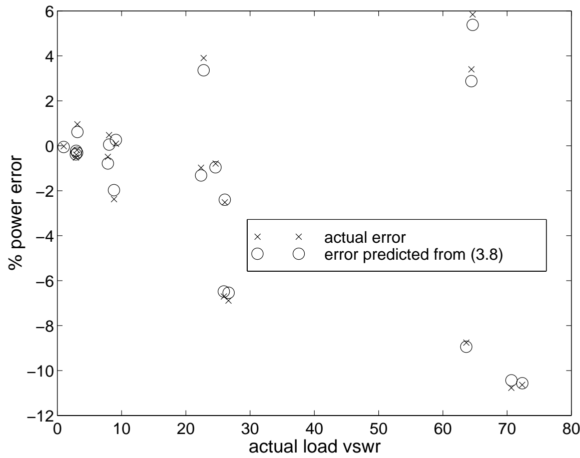

Figure 10: ϵ_P comparing $\widehat{P_{probe}}$ to P_{lrp} using voltage and current probe and HP8753 vector network analyzer

6 Error Modeling and Analysis

This section is motivated by an attempt to differentiate between the errors in $(\mathbf{V}^+, \mathbf{V}^-)$ and $(\mathbf{v}, \mathbf{i})$- based measurements. In the $(\mathbf{V}^+, \mathbf{V}^-)$- based measurement, simple de-embedding was sufficient to achieve $\pm 2\%$ error, but the same procedure only achieves $+6\%$ to -12% error in the $(\mathbf{v}, \mathbf{i})$- based measurement. Our goal is to propose a model for discussing measurement errors which allows us to think about error correction in a rigorous and structured manner. When we talk about the probe error, it makes sense to refer to how accurately it represents the state it 'sees'. Clearly it is unreasonable to assume that the probe can accurately measure the electrical state of the load if there is a highly lossy element with significant electrical length between it and the load. We see from (18) that small measurement errors result in large power errors. It is clear that neither probe measures the electrical state at either the input port or output port. Rather, both probes measure the electrical state at some point roughly in the middle of the probe. The difference in electrical state between the approximate middle of the probe and either input or output port is small, but the resulting error in power is likely to be significant. Accordingly, we will define the location at which the probe actually measures and define a model of the measurement system in Section 6.1. We will differentiate between the 'probe' and 'sensor' in the following manner. The probe is the physical device that connects to the transmission line. The sensor is that part of the probe which actually measures the electrical state, together with the data acquisition system.

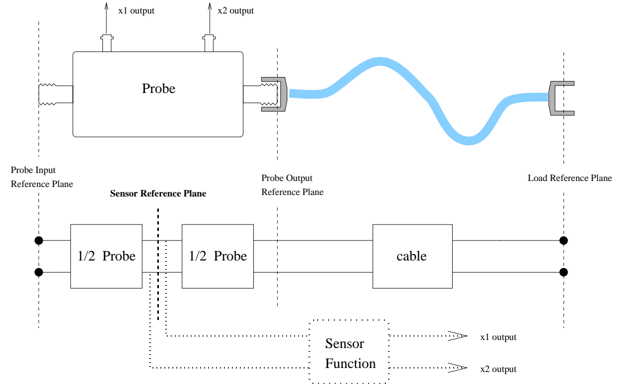

Figure 11: Probe Model Decomposition introducing the sensor reference plane

6.1 The Probe Network Model and Sensor Model

Figure 11 illustrates the proposed model. We introduce the *sensor reference plane*, defined as the location inside the probe where the measurment actually takes place. We introduce the sensor function as a model of the way the sensor processes the measurement. We need a sensor model because we observe that despite our best efforts, the electrical state at the sensor (x_{sensor}) does not relate exactly to the measured value ($\overline{x_{sensor}}$). Furthermore, we note that $\overline{x_{sensor}}$ changes as a function of our choice of data acquisition method, clearly indicating that the sensing function is completely independent of electrical network. For this reason, and because of its added flexibility, we choose to represent the sensing function as a simple transfer function relating the measured state ($\overline{x_{sensor}}$) to actual state (x_{sensor}). This approach allows us to describe the measurement process as the composition of two functions mapping the actual electrical state, x_{lrp}, to the measured state at the sensor reference plane $\overline{x_{srp}}$. First the state is mapped from the load reference plane to the sensor reference plane. Since this transformation follows the laws of network theory, it makes sense to represent it as an

ABCD matrix and use (27)

$$\begin{bmatrix} \mathbf{v}_{srp} \\ \mathbf{i}_{srp} \end{bmatrix} = \begin{bmatrix} A & B \\ C & D \end{bmatrix}_{lrp \to srp} \cdot \begin{bmatrix} \mathbf{v}_{lrp} \\ \mathbf{i}_{lrp} \end{bmatrix} \tag{27}$$

We should also note that since the transformation from $(\mathbf{V}^+, \mathbf{V}^-)$ to $(\mathbf{v}, \mathbf{i})$ is linear, we can easily express (27) in terms of $(\mathbf{V}^+, \mathbf{V}^-)$ by employing (1). The state that sensor 'sees' is obtained from (27). We then propose a function $\mathcal{F}_{sen}(x)$ which describes the map:

$$\overline{x_{srp}} = \mathcal{F}_{sen}(x_{srp})$$
$$\overline{x_{srp}} = \mathcal{F}_{sen}(\mathsf{A}_{lrp \to srp} \cdot x_{lrp}) \tag{28}$$

Given (approximate) knowledge of $\mathcal{F}_{sen}(x)$ and $\mathsf{A}_{lrp \to srp}$, we seek to invert these functions, apply them to the measured state and recover an estimate of the actual state, as shown in 29.

$$\widehat{x_{srp}} = \mathsf{A}^{-1}_{lrp \to srp} \cdot \mathcal{F}^{-1}_{sen}(\overline{x_{sensor}}) \tag{29}$$

Before leaving this section, we should note that the more complex sensor model presented in Figure 11 and 29 are compatible with standard calibration. If all we do is scale our measured values to engineering units and assume that the sensor reference plane is the load reference plane, what we are doing is proposing that $\mathcal{F}_{sen}(x)$ is simply (30),

$$\begin{bmatrix} \widehat{x_1} \\ \widehat{x_2} \end{bmatrix}_{srp} = \begin{bmatrix} K_{x_1} & 0 \\ 0 & K_{x_2} \end{bmatrix} \cdot \begin{bmatrix} \overline{x_1} \\ \overline{x_2} \end{bmatrix}_{lrp} \tag{30}$$

and that $\mathsf{A}^{-1}_{lrp \to srp}$ is simply the identity matrix. We have seen that this simple assumption about $\mathsf{A}^{-1}_{lrp \to srp}$ is not valid. We will now see that $\mathcal{F}_{sen}(x)$ proposed in 30 is inadequate as well.

6.2 Applying the Error Model to $(\mathbf{V}^+, \mathbf{V}^-)$ Data

Developing an exact model of $\mathsf{A}_{lrp \to srp}$ is not possible with our equipment. However, the assumption that the sensor reference plane is approximately at the mid point of the probe will be shown to yield good results. With this assumption, it is possible determine the model of the probe from the probe input reference plane or probe output reference plane to the sensor reference plane by a matrix square root of A_{probe}.

$$\mathsf{A}_{\frac{1}{2}probe} = \sqrt{\mathsf{A}_{probe}} \tag{31}$$

Using (31) combined with $\mathsf{A}_{prob_sys+xload}$ we can obtain the ABCD matrix to transform from the state at vector network analyzer port #2 to the state at the sensor reference plane with (32).

$$\mathsf{A}_{port2 \to srp} = \mathsf{A}^{-1}_{\frac{1}{2}probe} \cdot \mathsf{A}_{prob_sys+xload} \tag{32}$$

We then use this matrix in place of A_{xload} in (23) in order to convert from s_{21} to electrical state at sensor reference plane.

Plotting ϵ_P in Figure 12, we see that the $(\mathbf{V}^+, \mathbf{V}^-)$ based probe is in fact quite accurate. The measured value when using the HP8753 vector network analyzer to receive the probe's signal is almost exactly the actual state at the sensor reference plane. The vast majority of the 25% power error seen in Figure 7 is simply due to the fact that there is a lossy network between the sensor reference plane and load reference plane. Comparing of Figures 9 and 12 shows us that the de-embedded ϵ_P is slightly less than ϵ_P comparing $\overline{P_{srp}}$ to P_{srp}. This follows from the fact that the de-embedding procedure captures *both the probe network model and sensor model.*

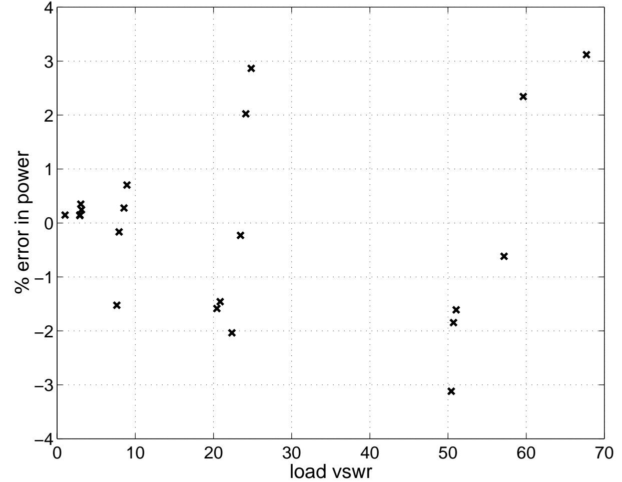

Figure 12: ϵ_P comparing $\overline{P_{srp}}$ to P_{srp} using Directional Coupler and HP8753 vector network analyzer

When we determine $\mathsf{A}_{\overline{probe}}$ using de-embedding, we are fitting a function from the class of linear, reciprocal two port networks to the map from state at the load reference plane to the state as measured by the sensor. This results from using the impedance calculated from *the probe's measurement of the state* and not the *actual impedance* at the load reference plane as the 'upstream' impedance. The advantage of the de-embedding model approach is that we have gained some accuracy over modeling only the network. In the case of the $(\mathbf{V}^+, \mathbf{V}^-)$- based measurement, the errors achieved with the de-embedding approach are sufficiently small not to require further investigation. This is not the case with the $(\mathbf{v}, \mathbf{i})$ based sensor.

6.3 Applying the Error Model to $(\mathbf{v}, \mathbf{i})$ Data

As we noted in section 5.2, the error after de-embedding of the $(\mathbf{v}, \mathbf{i})$ data is substantially higher than that of $(\mathbf{V}^+, \mathbf{V}^-)$ data. Given this fact, Figure 13, showing ϵ_P at the sensor reference plane is no surprise. Given that a linear correction is insufficient, we must consider a nonlinear correction. Since the probe network is by definition constructed of linear network elements, we must look elsewhere for a source of non linear errors.

The most compelling mechanism for nonlinear measurement behavior has to do with the way $(\mathbf{V}^+, \mathbf{V}^-)$ and $(\mathbf{v}, \mathbf{i})$ quantities behave at high VSWR. In $(\mathbf{V}^+, \mathbf{V}^-)$- based measurement under the test conditions we have designed, $\mid \mathbf{V}^+ \mid$ is constant very near the value at which we calibrated $K_{\mathbf{V}^+}$. As VSWR increases, so does $\mid \mathbf{V}^- \mid$, approaching the value at which we calibrated $K_{\mathbf{V}^-}$. Figure 14 shows why the simple model we assumed in Section 4.5 works so well with the experiment we performed: as accuracy becomes increasingly critical, the quan-

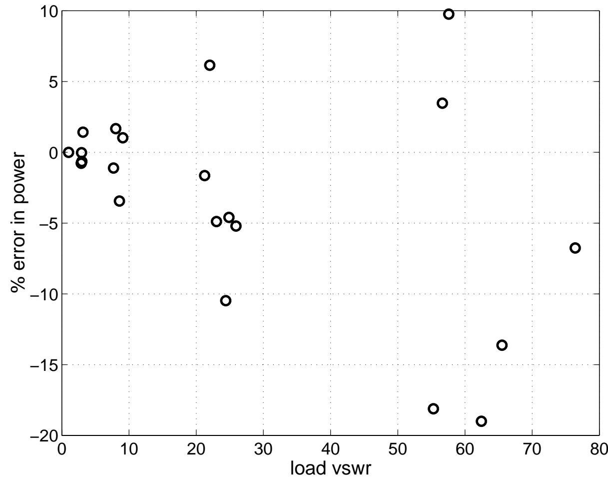

Figure 13: ϵ_P comparing $\overline{P_{srp}}$ to P_{srp} using Current and Voltage based Probe and HP8753 vector network analyzer

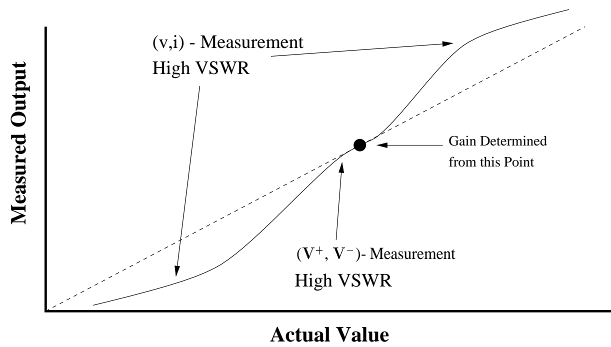

Figure 14: Calibration gain as a local linearization of the $\mathcal{F}_{sen}(x)$ map

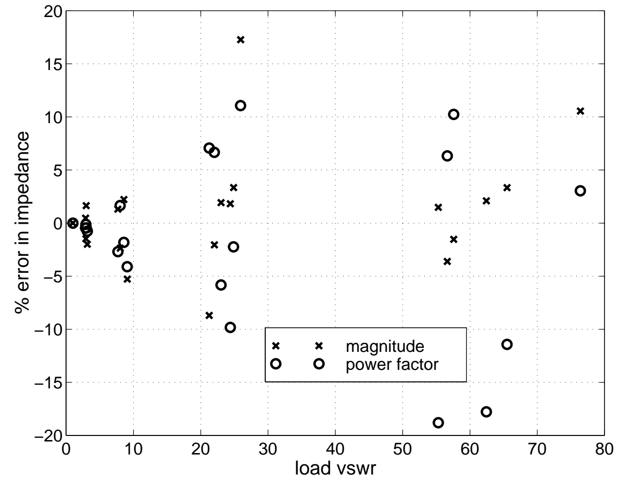

Figure 15: $\epsilon_{\mathbf{Z}_{srp}}$ and $\epsilon_{\theta_{Z_{srp}}}$ comparing $\widehat{\mathbf{Z}_{srp}}$ to $\mathbf{Z}_{srp}$ using Current and Voltage based Probe and HP8753 vector network analyzer

tities we need to know approach the point where we know them most accurately. The situation is not the same in $(\mathbf{v}, \mathbf{i})$ based measurement. As VSWR increases, one or all three of the quantities we need to know: $|\ \mathbf{v}\ |, |\ \mathbf{i}\ |$, and θ_Z deviates substantially from the calibration value. One of the magnitudes gets small, the other gets large, and the phase strays from 0. Figure 14 shows this effect. As our need for accuracy increases, at least one of our quantities strays from the 'operating point': the point we use for our linear approximation of $\mathcal{F}_{sen}(x)$.

Development of a nonlinear error correction is greatly simplified by finding correlation in the data. Figure 15 shows the error in $(\mathbf{v}, \mathbf{i})$- based electrical state at the sensor reference plane. Finding a correlation in the data is achieved by a relatively straight forward but tedious process of plotting the sources of error as a function of measured electrical state. The the most succesful fitting functions take the form of a nonlinear gain term in $\overline{\phi_\Gamma}$ as shown in 33.

$$\widehat{x_{srp}} = (k_1 + k_2(\overline{\phi_{\Gamma_{srp}}}) + k_3(\overline{\phi_{\Gamma_{srp}}})^2 \ldots k_n(\overline{\phi_{\Gamma_{srp}}})^{n-1})\overline{x_{srp}} \quad (33)$$

A second order polynomial fit can be used to correct the $\overline{\theta_Z}$ data. Since both $|\ \mathbf{v}\ |$ and $|\ \mathbf{i}\ |$ have a sharp increase in error with $\overline{\phi_{\Gamma_{srp}}}$, a 9th order polynomial is used. Such a high order function could be avoided by using a trigonometric function of $\overline{\phi_{\Gamma_{srp}}}$, which would 'stretch' the region of high magnitude sensitivity.

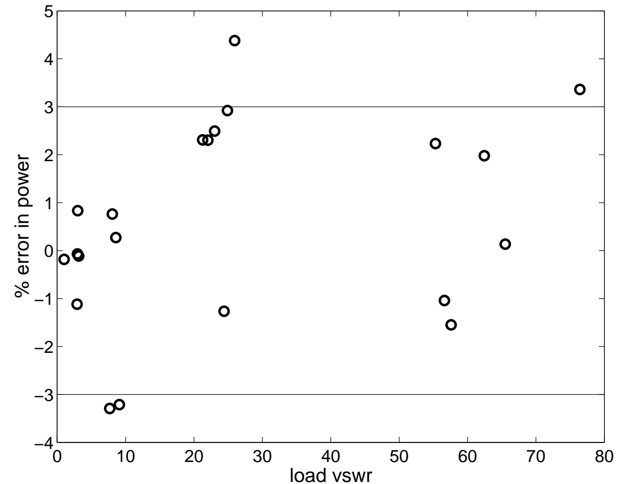

Figure 16: ϵ_P comparing nonlinear $\widehat{P_{srp}}$ to P_{srp} using Current and Voltage based Probe and HP8753 vector network analyzer

Figure 16 shows the results of applying the nonlinear gain of (33) to the $(\mathbf{v}, \mathbf{i})$ data. With the exception of a few points, the data is within $\pm 3\%$ power error. This presents a substantial improvement over the actual data at the sensor reference plane, and the results achieved using the linear 'de-embedding' algorithm. The fit was achieved using about $\frac{1}{3}$ of the data points, and the results shown in Figure 16 are for the whole data set. Although certainly not conclusive, this suggests a globally valid identification function. Although data at the load reference plane is not presented, transforming from sensor reference plane to load reference plane is simple linear function which will have no impact on the results of Figure 16.

Figure 16 shows we have achieved one of the stated premises of this paper. Our data indicates that the performance at the sensor reference plane of the ($\mathbf{V}^+$, $\mathbf{V}^-$)- based sensor is superior to that of the ($\mathbf{v}$, $\mathbf{i}$)- based sensor. However, with the application of known identification techniques, we can develop a model of the sensor behavior and achieve roughly equivalent results after correction.

7 Conclusions

The theoretical derivation of power error as a function of measurement error is well supported by experimental data for both ($\mathbf{V}^+$, $\mathbf{V}^-$) based and ($\mathbf{v}$, $\mathbf{i}$) based measurments. This relationship states that at high load VSWR's, often found in typical plasma operating conditions, reasonable power accuracy, on the order of $\pm 5\%$ requires extreme measurement accuracy, on the order of $\pm 0.05\%$. This type of accuracy is only feasible on research - grade data acquisition equipment combined with the use of linear model based sensing in the case of ($\mathbf{V}^+$, $\mathbf{V}^-$) based measurment and nonlinear model based sensing in the case of ($\mathbf{v}$, $\mathbf{i}$) based measurment. It remains to be seen what kind of accuracy is possible with commercially viable, real time compatible data acquisition systems.

Acknowledgments

The authors would like to thank Professor Valdis V. Liepa for use of his equipment and Shawn Ohler, Sven Bilén, Sanjay Raman, and Daniel Zahn for their assistance with equipment, calibration and measurement technique.

This work supported in part by AFOSR/ARPA MURI Center under grant # F49620-95-1-0524 and The Semiconductor Research Company under contract #96-FC-085.

References

[1] V. A. Godyak, R. B. Piejak, and B. M. Alexandrovich, IEEE Transactions on Plasma Sciences **19**, 660 (1991).

[2] B. Andries, G. Ravel, and L. Peccoud, J. Vac. Sci. Technol. A **7**, 2774 (1989).

[3] J. W. Butterbaugh, L. D. Baston, and H. H. Sawin, J. Vac. Sci. Technol. A **8**, 916 (1990).

[4] P. Rummel, in *Proceedings of SPIE* (International Society for Optical Engineering, Bellingham, Washington, 1991), Vol. 1392, pp. 411–420.

[5] G. C. Zau, J. W. Butterbaugh, P. Rummel, and H. H. Sawin, J. Electrochem. Soc. **138**, 872 (1991).

[6] F. Bose, R. Patrick, and H. Baltes, in *Manufacturing Process Control for Microelectronic Devices and Circuits* (International Society for Optical Engineering, Bellingham, Washington, 1994), Vol. 2336, pp. 101–110.

[7] J. H. Keller and W. B. Pennebaker, IBM J. Res. Develop. **23**, 3 (1979).

[8] W. B. Pennebaker, IBM J. Res. Develop. **23**, 16 (1979).

[9] A. J. vanRoosmalen, W. G. M. van den Hoek, and H. Kalter, J. Appl. Phys. **58**, 653 (1985).

[10] A. Pananjpe, J. P. McVittie, and S. A. Self, J. Appl. Phys. **67**, 6718 (1990).

[11] V. A. Godyak, R. B. Piejak, and B. M. Alexandrovich, J. Appl. Phys. **69**, 3455 (1991).

[12] V. A. Godyak and R. B. Piejak, J. Vac. Sci. Technol. A **8**, 3833 (1990).

[13] H. Shan, Ph.D. thesis, Stanford University, 1991.

[14] M. Klick, J. Appl. Phys. **79**, 3445 (1996).

[15] S. Bushman, T. F. Edgar, and I. Trachtenberg, in 185th *Electrochemical Society Meeting, Tenth Symposium on Plasma Processing* (Electrochemical Society, Bellingham, Washington, 1994), Vol. 185, pp. Pennington, New Jersey.

[16] S. Bushman, T. F. Edgar, I. Trachtenberg, and N. Williams, in *Proceedings of SPIE* (International Society for Optical Engineering, Bellingham, Washington, 1994), Vol. 2336.

[17] W. C. Roth, Master's thesis, University of Arizona, 1995.

[18] M. A. Sobolewski, J. Res. Natl. Inst. Stand. Technol. **100**, 341 (1995).

[19] M. A. Sobolewski, J. Vac. Sci. Technol. A **10**, 3550 (1992).

[20] J. Hargis, P. J. *et al.*, Rev. Sci. Inst. **65**, 140 (1994).

[21] D. M. Pozar, *Microwave Engineering* (Addison-Wesley, Reading, Massachusets, 1993).

[22] A. J. Miranda, Master's thesis, University of California at Berkely, 1995.